Circularly polarised luminescence bioimaging using chiral BODIPYs: A model scaffold for advancing unprecedented CPL microscopy using small full-organic probes

Patrycja Stachelek,[a] Sergio Serrano-Buitrago,[b] Beatriz L. Maroto,[b] Robert Pal,*[a] Santiago de la Moya.*[b]

[a] Dr. P. Stachelek, Prof. Dr. R. Pal, Department of Chemistry, Durham University, Stockton Road, Durham DH1 3LE, Durham, United Kingdom.

E-mail: robert.pal@durham.ac.uk

[b] S. Serrano-Buitrago, Prof. Dr. B. L. Maroto, Prof. Dr. S. de la Moya, Departamento de Química Orgánica, Facultad de, Ciencias Químicas, Universidad Complutense de Madrid, Ciudad Universitaria, s/n, 28040, Madrid, Spain

E-mail: santmoya@ucm.es

KEYWORDS: Circularly polarised luminescence • Laser scanning confocal microscopy • CPL probes • BODIPY • Bioimaging

ABSTRACT: Unprecedented circularly polarised luminescence bioimaging (CPL-bioimaging) of live cells using small full-organic probes is firstly reported. These highly biocompatible and adaptable probes are pivotal to advance emerging CPL Laser-Scanning Confocal Microscopy (CPL-LSCM), as an undeniable tool to distinguish, monitor and understand the role of chirality in the biological processes. The development of these probes was challenging due the poor dichroic character associated to the involved CPL emissions. However, the known capability of the BODIPY dyes to be tuned to act as efficient fluorescence bioprobes, joint to the capability of the BINOL-*O*-BODIPY scaffold to enable CPL, allowed the successful design of the first examples of this kind of CPL probes. Interestingly, the developed CPL probes were also multiphoton (MP) active, paving the way for envisioned MP-CPL-bioimaging. The described full-organic CPL-probe scaffold, based on an optically and biologically tunable BODIPY core, which is chirally perturbed by an enantiopure BINOL moiety, represents therefore a simple and readily accessible structural design for advancing efficient CPL probes for bioimaging by CPL-LSCM.

INTRODUCTION

Most building blocks of Nature, such as amino acids and sugars, are chiral, therefore, probing the interactions of these molecules, and/or tracking their origin and fate in living organisms is of great importance in both biology and medicine.[1] For instance, even though both enantiomeric versions (L and D) of the chiral natural amino acids exist, all life on Earth is based on the L enantiomers. Thus, understanding the origins of Nature´s homochirality and the key roles played by it within living systems is of key importance.

Luminescent chiral emitters, like chiral BODIPYs (boron dipyrromethenes) **BOD1-3** presented here in Fig. 1, display a unique optical fingerprint, their emitted circularly polarised light. This circularly polarised luminescence (CPL) can be used to carry information about the chiral molecular environment, as well as about the conformation and binding state of the chiral CPL emitter (*i.e.*, the CPL probe). Although in the last few decades there has been a surge in the development of chiral molecules, complexes and polymers as CPL emitters, the technological advancements to characterize the CPL signal coming from these luminescent entities in complex environments, like the biological ones, were stagnant.

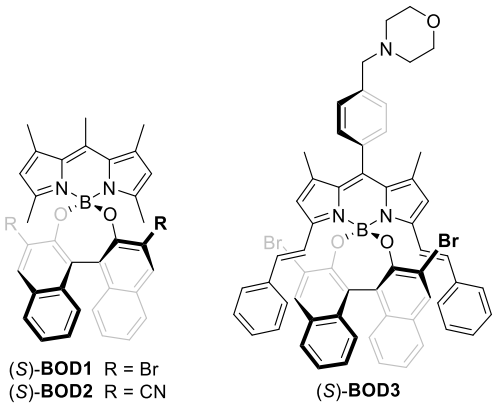

Figure 1. Small full-organic CPL probes based on BINOL-*O*-BODIPY (**BOD1-3**). Only the *S* enantiomers are depicted.

CPL spectroscopy is a well-established technique, with CPL emission maximized for electronic transitions that are magnetic-dipole allowed and electric-dipole forbidden. CPL emission is most commonly quantified in terms of the emission dissymmetry factor, g_{lum},

as defined by Eqn. 1, where I_L and I_R are the intensities of the emitted left- and right-handed CPL (L-CPL and R-CPL, respectively). Thus, $g_{lum} = +2$ indicates 100% L-CPL emission, $g_{lum} = -2$ indicates 100% R-CPL emission, and $g_{lum} = 0$ indicates net-zero circular polarisation in the emitted light. The strongest CPL signals to date have been generated from purpose engineered chiral lanthanide coordination complexes, specifically europium complexes, exhibiting $|g_{lum}|$ up to 1.38 for simple systems, and up to 1.45 for chiral supramolecular polymers.[2]

$$g_{lum} = \frac{2(I_L - I_R)}{(I_L + I_R)} \qquad \text{Eqn. 1}$$

Triggered by the development of CPL emitters in recent years, there have been significant advancements in CPL instrumentation and techniques, including solid-state time-resolved CPL spectrometers,[3] CPL photography,[4] and CPL-Laser Scanning Confocal Microscopy (CPL-LSCM).[5] CPL-LSCM represents a particularly exciting development, as it enables us, for the first time, to probe the chiral subcellular environment using CPL probes, offering a unique opportunity to investigate how different enantiomers can differently interact with other chiral biomolecules and molecular systems within cells.[5]

For efficient excitation and detection with CPL-LSCM, the CPL probe used must possess a high molar absorption coefficient (ξ_{abs}), along with a favourable photoluminescence quantum yield (ϕ_{em}) and a significant g_{lum} value. This can be quantified by the Circularly Polarised Brightness (*CPB*) (Eqn. 2), which serves as a comparative metric for the total number of circularly polarised photons emitted and, therefore, acts as the figure-of-merit to compare CPL emitters.[2,6]

$$CPB = \xi_{abs}\phi_{em}\left(\frac{|g_{lum}|}{2}\right) \qquad \text{Eqn. 2}$$

The capability of CPL-LSCM to enable CPL-based bioimaging (CPL-bioimaging) of cell systems, by differentially detecting simultaneous L-CPL and R-CPL emissions by Enantioselective Differential Chiral Contrast (EDCC) imaging, has been recently demonstrated by us using purpose-engineered CPL probes based on chiral lanthanide complexes exhibiting both high $|g_{lum}|$ and high *CPB*.[5] These CPL probes have shown the potential of CPL-LSCM imaging technology to study key diastereomeric interactions taking place in the living systems, as those enabling the observed differential accumulation of the used CPL-probe enantiomers in different cell organelles.

A step forward in the use of CPL-LSCM is to image biological systems by using small full-organic CPL probes. Fluorescent small full-organic probes are commonly used in bioimaging by fluorescence microscopy due to key advantages derived from their organic nature and small size, such a high capability for cell-membrane permeation, notable biocompatibility, or easy adaptability by workable organic chemistry.[7] In this context, pioneering small full-organic CPL probes should pave the way for unprecedented studies on the role played by chirality in the biological processes, based on more accurate and biocompatible CPL-bioimaging experiments using CPL-LSCM. However, the design of these probes is challenging, since a precise molecular engineering of a small organic chromophoric scaffold is needed to achieve the required proper *CPB* without losing biocompatibility and organelle selectivity. Specifically, achieving favourable *CPB* values is highly demanding due to the poor $|g_{lum}|$ values of the small organic chiral molecules, falling within the 10^{-4}–10^{-3} interval in most of the cases.[8] To face this challenge, pioneering the first workable small full-organic CPL probes, we selected the small full-organic BODIPY (boron dipyrromethene) chromophoric scaffold.

BODIPYs have been chosen for the development of a plethora of light-triggered applications and tools.[9,10] The main strength of the BODIPYs relate to their high fluorescence brightness, facile synthesis, and easy adaptability by a number of well-known BODIPY chemical transformations (BODIPY chemistry),[11,12] including derivatisations at the boron atom.[13] This adaptability includes the position of the emission bands (*e.g.*, from *ca.* 395 nm for the 8-aminoBODIPYs reported by Bañuelos *et al.*[14], to *ca.* 910 nm for the π-extended BODIPYs reported by Harriman *et al.*[11,15]), the possibility of enabling efficient, selective bioprobing,[16,17] or the possibility of enabling efficient CPL.[18]

On the basis of the high adaptability of the BODIPYs, herein we report the design, synthesis and CPL-bioimaging capability of enantiopure (*R*)- and (*S*)-**BOD1-3** (Fig. 1), as the first small full-organic CPL probes enabling CPL bioimaging by CPL-LSCM. These CPL probes are based on the readily-accessible CPL-enabling BINOL-*O*-BODIPY scaffold (BODIPY functionalized at boron with a 1,1′-bi-2-naphthol moiety).[19]

Results and Discussion

As above mentioned, to pioneer the first small and full-organic probes for CPL-bioimaging we selected the chiral BINOL-*O*-BODIPY scaffold. This selection was made on the known potential of this scaffold to rapidly develop small and full-organic CPL emitters from readily available both *F*-BODIPYs (4,4-difluoro-BODIPYs) and enantiopure BINOLs.[19–23] The restricted conformational mobility of the BINOL moiety in these dyes (*e.g.*, see in Fig. 1) is key to assure CPL emission with significant $|g_{lum}|$ value from the inherently achiral BODIPY chromophore,[19] whereas their fluorescent capabilities can be strongly enhanced by properly selecting the substituents at both the BODIPY and the BINOL moieties, in order to diminish BINOL-to-BODIPY charge transfer,[20,24–27] as well as internal conversion by conformational mobility.[28] The selection of the BINOL-*O*-BODIPY scaffold was also made with consideration for the potential to achieve photostable dyes under the severe laser irradiation required by CPL-LSCM, as well as its recently demonstrated capability to generate efficient fluorescent bioprobes in living mammalian cells, due to their high biocompatibility and ease for permeating cell membranes.[22]

Synthesis

Harnessing the above-mentioned advantages of the BINOL-*O*-BODIPY scaffold, we selected the known BINOL-*O*-BODIPY-based fluorescent bioprobes **BOD1** and **BOD2** (see Fig. 1)[22] to investigate the possibility of detecting the expected weak, green CPL signals coming from the marked cell organelle (lipid droplets and lysosomes, respectively), using CPL-LSCM.

For this purpose, and also to test possible diastereomeric effects similar to those described when using lanthanide-complex CPL-probes,[5] we synthesized the two enantiomers of each probe from commercial 1,3,5,7,8-pentamethyl-*F*-BODIPY and the corresponding enantiopure BINOL. This was made following the described synthetic procedures.[22,25]

Additionally, in order to explore the potential of the BINOL-*O*-BODIPY scaffold to rapidly develop CPL probes, we synthesized both enantiomers of **BOD3** (see Fig. 1), which was rationally designed to act as an efficient red-fluorescent CPL probe for lysosomes. Thus, **BOD3** is based on 1,3,5,7-tetramethyl-*F*-BODIPY (**FB1**) (see Scheme 1), which is a known, efficient green-fluorescent lysosome probe (note the presence of the basic morpholine moiety promoting its accumulation into acidic lysosomes).[29]

For **BOD3** preparation, we firstly synthesized **FB1** according to the known procedure,[29] and then extended the BODIPY-chromophore π conjugation to enable emission in the red region. This π-extension was done by well-known Knoevenagel-like distyrylation in 3,5-dimethylBODIPYs (see Scheme 1).[30] The obtained red-emitting *F*-BODIPY **FB2** was then endowed with CPL capability by standard at-boron BODIPY BINOLation.[19] This BINOLation was done using the marketed enantiomers of 3,3´-dibromoBINOL to construct the corresponding BINOL-*O*-BODIPY enantiomers **BOD3** (see Scheme 1).

Scheme 1. Synthesis of red BINOL-*O*-BODIPY BOD3 (exemplified for the *S* enantiomer) as a red-fluorescent lysosome CPL probe.

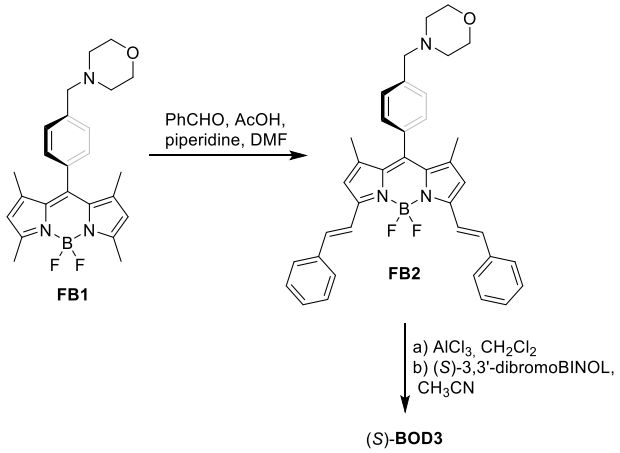

CPL spectroscopy

Firstly, we verified the CPL activity of **BOD1-2** enantiomers by CPL spectroscopy.[31] As expected, the corresponding enantiomers displayed weak mirror-image visible dichroic signals in diluted chloroform solution (see Fig. S1 in the SI). The calculated small g_{lum} values (Table 1) are in line with the typical values found for other enantiopure BINOL-*O*-BODIPYs.[19-21,23] Despite these small values, we trusted to take advantage of the known, high fluorescence efficiencies of **BOD1-2** (see ϕ_{em} values in Table 1),[22] enabling the consecution of a moderate *CPB* value for **BOD1** (*ca.* 12 $M^{-1}cm^{-1}$ in chloroform solution; see Table 1).

Expectedly, photoluminescent (PL) and CPL spectroscopies of unprecedented **BOD3** demonstrated chir(optical) behaviours comparable to those exhibited by **BOD1-2** (see Table 1, and Figs. S1 and S2 in the SI), and related distyrylated BINOL-*O*-BODIPYs,[19-21,23] resulting in a relatively high *CPB* value (*ca.* 34 $M^{-1}cm^{-1}$ in chloroform solution; see Table 1).

The different *CPB* values recorded for **BOD1-3** in solution support their use to investigate the possibility of CPL-bioimaging live cells by small full-organic CPL probes using CPL-LSCM.

CPL-bioimaging of live cells

To test the capability of **BOD1-3** to act as a small full-organic CPL probes enabling bioimaging using the CPL-LSCM, NIH 3T3 (mouse skin fibroblast, ATCC-CRL-1658) cells were selected and dosed with 10 μM of the corresponding BODIPY dye enantiomer for 24 h incubation time.

After initial imaging experiments with 5 μM dosing concentration, we found that the probe concentration needed to be increased at least two-fold in order to obtain desirable brightness, especially when using selective narrow wavelength range bandpass (BP) filters. This is in agreement with both the small $|g_{lum}|$ values and the modest *CPB* values of the small full-organic **BOD1-3** when compared to the seminal lanthanide-complex CPL probes.[2,5]

Interestingly, despite the *CPB* values of **BOD1-3** are significantly lower than those of the lanthanide-complex CPL probes,[5] it was possible to record CPL signals from cells with the used concentrations. Noteworthy, **BOD1-3** did not trigger cytotoxicity to the naked eye (cell morphology changes) under the selected probe concentration, staining conditions and imaging protocol.

The resulting CPL-based images were analysed using EDCC protocols as introduced by Frawley *et al.*,[32] and further developed by Stachelek *et al.* and De Rosa *et al*.[4,5] In brief, EDCC imaging is realized by subtraction of the simultaneously recorded L-CPL image from the R-CPL one (and vice versa). This was done using ImageJ software (v1.49),[4,5] and it allows determining whether the major CPL component consists of L-CPL or R-CPL.

To our pleasure, we were able to record R-CPL and L-CPL images of lipid droplets in living NIH 3T3 cells by using small full-organic (*S*)-**BOD1** as the CPL probe (see Fig. 2). The L-CPL images were of higher contrast (*cf.* Figs. 2B and 2C) in agreement with the positive sign of the CPL emission of (*S*)-**BOD1** in solution (see Table 1), corresponding to preferential emission of L-CPL. However, this imaging contrast is striking when considering the small $|g_{lum}|$ value exhibited by (*S*)-**BOD1** in solution (see Table 1), which anticipates almost identical R-CPL (Fig. 2B) and L-CPL-based (Fig. 2C) images. We suggest that chiral amplification *in cellulo* could be behind this observation. Thus, the recorded CPL signal, coming from the BINOL-*O*-BODIPY probe, could be amplified by the local cell environment, helically-chiral organized due to "the Sergeants and Soldiers principle".[33,34] Thus, close abundant molecules in the biological environment (*e.g.*, lipids) could be helically organized with a preferred helical configuration induced by the enantiopure chiral probe (chiral templating), enabling the amplification of the CPL signal. Nevertheless, this is still a relatively unexplored area of science that has to date focused on the synthesis of the chiral materials used as CPL bioprobes, and requires more insight to

Table 1. Key (chir)optical signatures of small full-organic (*S*)-BOD1-3 recorded from diluted $CHCl_3$ solution (*ca.* 10^{-6} M). Data for the corresponding (*R*) enantiomers are almost identical, with the exception of the g_{lum} sign.

probe	λ_{abs} / nm	ξ_{abs} / $M^{-1}cm^{-1}$	λ_{em} / nm	ϕ_{em}	g_{lum}	CPB (λ_{em}) / $M^{-1}cm^{-1}$
(*S*)-BOD1	503.0[a]	66 000[a]	528.5[a]	0.620[a]	$+6.0 \times 10^{-4}$	12.3 (528.5 nm)
(*S*)-BOD2	503.0[a]	50 800[a]	529.0[a]	0.870[a]	$+2.0 \times 10^{-4}$	4.4 (529.0 nm)
(*S*)-BOD3	635.0	64 000	653.0	0.770	$+1.4 \times 10^{-3}$	34.5 (653.0 nm)

[a]Data collected from ref. 22.

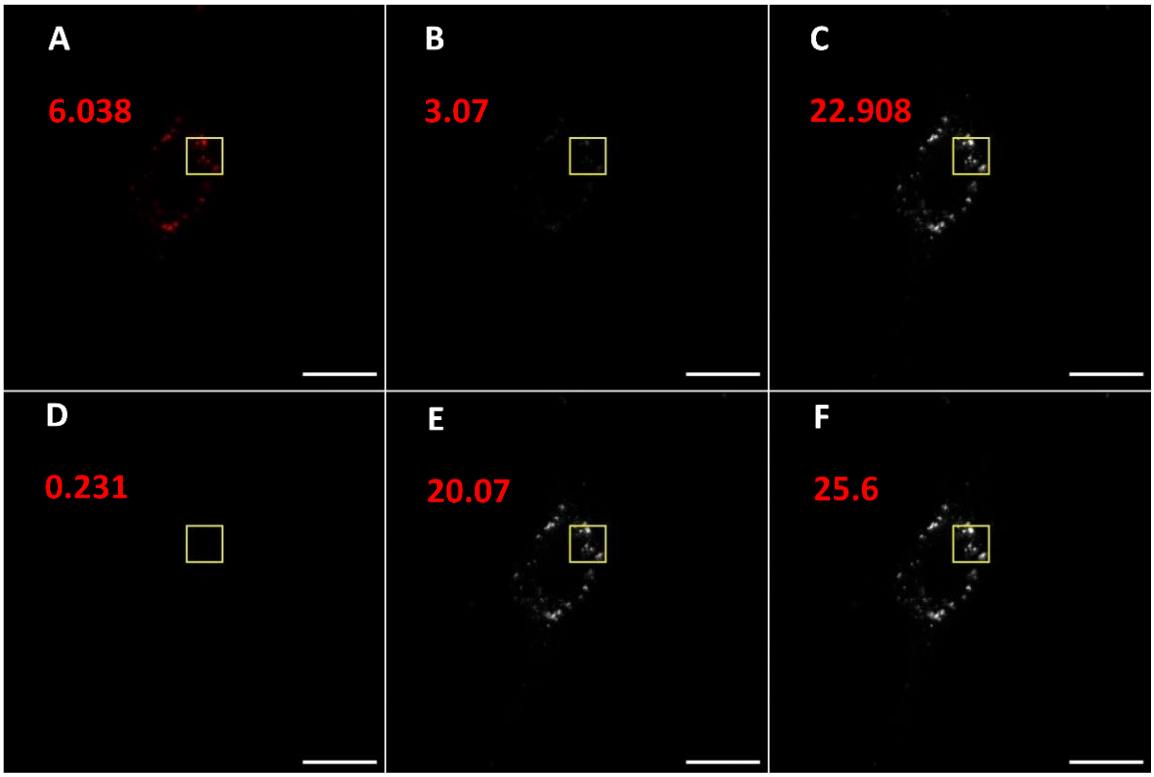

Figure 2. First CPL-bioimaging using a small full-organic CPL probe. Localisation of enantiopure (*S*)-**BOD1** in living NIH 3T3 cells by LSCM (**A**), CPL-LSCM (**B** and **C**) and CPL-LSCM/EDCC (**D** and **E**) (10 µM, 24 h loading, ×631.4 NA oil objective, 96 × 96 µm FOV, 100 avg., 790 nm axial section). **A**: Total-emission LSCM image (λ_{ex} = 355 nm, 20 mW; λ_{em} = 570–800 nm). **B** and **C**: R- and L-CPL-LSCM images obtained by using the R- and L-CPL channel, respectively (λ_{ex} = 355 nm, 20 mW; λ_{em} = 589–599 nm). **D**: Right – Left EDCC. **E**: Left – Right EDCC. **F**: **B**+**C** merged image. Scale bars = 20 µm. Numbers in red are avg. 8-bit pixel intensity values for each image region.

obtain in-depth understanding of the amplification of chirality by chiral templating in cells.[35-37] Interestingly, no change in the intracellular localisation of the probe was detected when using (*R*)**-** instead of (*S*)**-BOD1**, and only the contrast of the corresponding R-CPL- and L-CPL-based images was switched (*cf.* Fig. 2, and Fig. S3 in the SI).

Analogously, we were also able to record R-CPL- and L-CPL-based images of lysosomes in living NIH 3T3 cells by selecting green-emitting (*R*)- or (*S*)-**BOD2** (see Figs. S4 and S5 in the SI), or by selecting red-emitting (*R*)- or (*S*)-**BOD3** as the CPL probe (see Fig. S6 and S7 in the SI). Once again, the L-CPL images were recorded with higher contrast for the *S* enantiomers, and vice versa, in agreement with the signs of the CPL emissions of the enantiomers in solution (see Table 1).

The obtained CPL-based images (Figs. 2, and Figs S3-S7 in the SI) confirm that CPL-LSCM can be applied to CPL-image living systems with small full-organic CPL probes exhibiting small CPL brightness, even as small as *ca.* 4 $M^{-1}cm^{-1}$, under reasonable probe concentrations (around 10 µM) and incubation times (*ca.* 24 h), and despite the very small $|g_{lum}|$ values (*ca.* 0.001) displayed by this kind of CPL probes (small full-organic molecular emitters). Moreover, they demonstrate the capability of the chiral BINOL-*O*-BODIPY scaffold to rapidly develop specific CPL

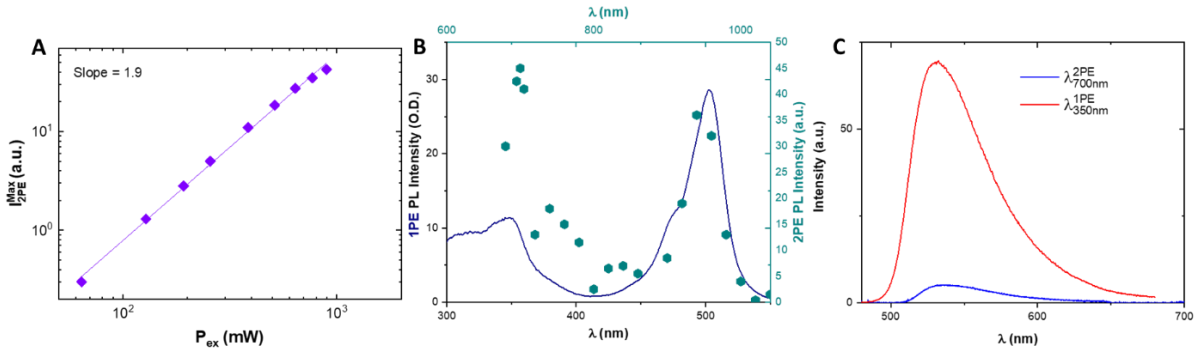

Figure 3. Key 2P-activity parameters and spectra of **BOD1** in chloroform. **A**: Excitation power dependency of the 2P-induced emission (2PE) intensity (slope 1.9 ± 0.1; σ^2 = 21 ± 3 GM). **B**: One-photon excitation (λ_{em} = 527 nm, solid blue line) and two-photon excitation (λ_{em} = 527 nm, dark cyan dots) spectra. **C**: One- (λ_{ex} = 350 nm, solid red line) and two-photon induced (λ_{ex} = 700 nm, solid blue line) emission spectra of **BOD1**.

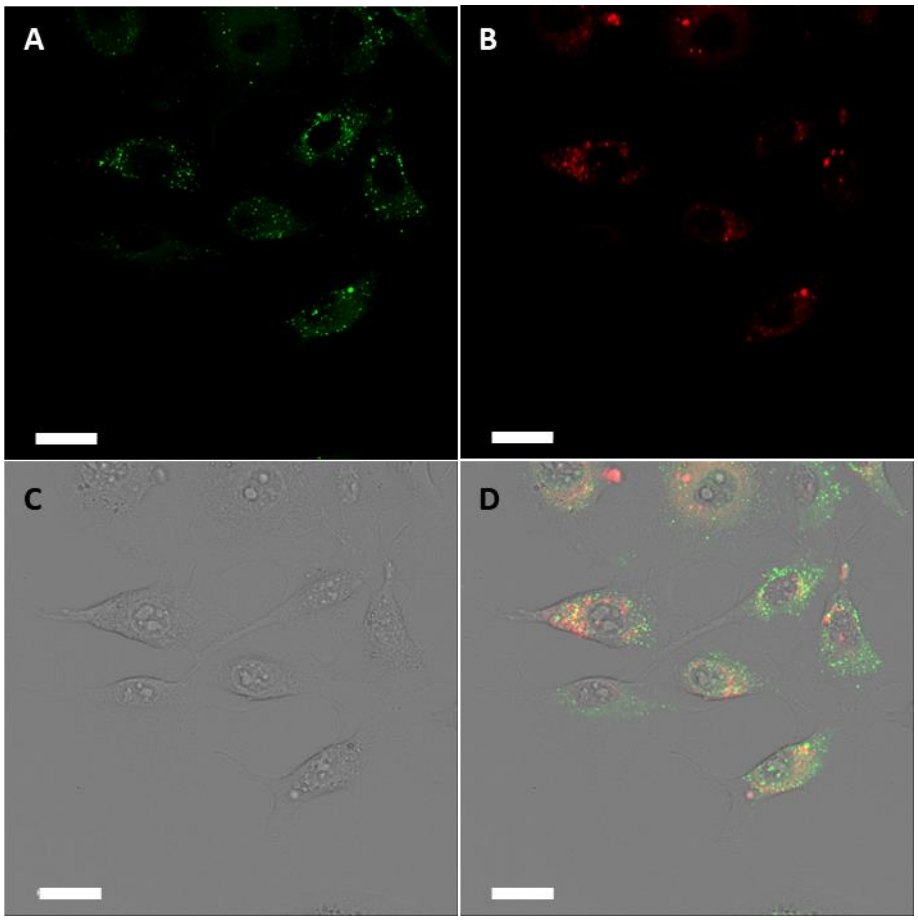

Figure 4. Localisation of enantiopure (*S*)-**BOD1** (5 µM) in living NIH 3T3 cells. **A**: LSCM image (λ_{ex} = 488 nm, 6 mW; λ_{em} = 500–600 nm). **B**: Two-photon fluorescence image (λ_{ex} = 960 nm, 36 mW; λ_{em} = 500–600nm). **C**: Transmission image (λ_{ex} = 488 nm). **D**: **A**+**B**+**C** images merged (calculated Pearson´s coefficient = 0.73). Scale bar = 20 µm.

probes (with different probing behavior, different positions of the key spectral bands, and different CPL signs), for CPL imaging.

Multiphoton activity

The BINOL-*O*-BODIPYs presented herein were purpose designed for CPL-bioimaging, hence we endeavoured to test whether they are multiphoton (MP) active. It must be noted that MP microscopy techniques reduce cellular phototoxicity by harnessing a tightly focused biologically safe near infrared laser pulse (typically

femtoseconds) to stimulate emission from fluorescent molecules that would otherwise require absorption of a single high-energy ultraviolet photon. The tightly defined spatial constraints of MP microscopy additionally offers both improved axial (z-axis) resolution and sub-cellular sectioning capability for imaging, as well as enhanced tissue penetration for photodynamic therapy applications.[38-40] For efficient two-photon excitation, the probe must have a high two-photon absorption (2PA) cross section (σ^2) (typically 100−1000 GM; 1 GM = 10^{-50} cm^4 s $photon^{-1}$) with a favourable emission quantum yield.[40]

To our satisfaction, we were able to determine the σ^2 values of **BOD1-3** according to established procedures (σ^2 = 21 ± 3 GM, 12 ± 3 GM, and 17 ± 3 GM respectively, in chloroform).[5] Unfortunately, these σ^2 values are relatively small when compared to those recorded previously for *F*-BODIPY dyes.[41] As an example, Fig. 3 shows the key MP signatures of **BOD1** (for **BOD2** and **BOD3** see Figs. S8 and S9 in the SI).

MP event due to 2PA was verified by the quadratic dependence of the recorded maximum-emission intensity (I^{max}_{2PE}) on the excitation power (P_{ex}) (*e.g.*, see Fig. 3A for **BOD1**). It is important to note that, due to the involved nonlinear effect (non-degenerate two-photon absorption), the wavelength of the 2PA-enabled excitation-spectrum main band is lower than the expected, and extremely rarely double of the 1PA-enabled excitation-spectrum maximum (*e.g.*, see Fig. 3B for **BOD1**). This is especially true for organic compounds.[42] Moreover, due to the quadratic relationship between the intensity of the 2PA excitation and the triggering of a fluorescent event, the shape of 2PA-induced emission band is inherently always far narrower, and also sharper than the obtained by 1PA excitation (*e.g.*, see Fig. 3C for **BOD1**).

The collected MP spectroscopy results suggest that our BINOL-*O*-BODIPY-based CPL probes could be excited with physiologically safer NIR to bioimaging purposes.[39] Indeed, in spite of the small σ^2 values determined for these probes, we were able to bioimage lipid droplets by dosing live NIH 3T3 cells with 5 μM of **BOD1**, under 2PA NIR excitation at 960 nm (Fig. 4). However, it is important to note that the determined σ^2 values are on the lower end of the spectrum of values for workable MP probes.[43-45] This fact coupled with the small $|g_{lum}|$ and modest *CPB* values of **BOD1-3** make them unlikely candidates to act as workable CPL probes for MP-CPL-bioimaging, and superior full-organic small probes should be designed for investigating this possibility.

CONCLUSION

It is demonstrated that the small $|g_{lum}|$ values associated to the CPL emission of the small full-organic chiral molecules are not necessarily a limitation for CPL-bioimaging when these materials are used as CPL probes. Thus, only moderate *CPB* values seem to be needed, which can be easily achieved due to the high fluorescence efficiencies of these materials.

It is encouraging that the associated imaging technique and protocol (CPL-LSCM) is able to utilize the weak CPL emission from the small full-organic chiral emitters to obtain CPL-based bioimages of high quality and contrast. We suggest that chiral amplification by chiral templating of abundant biomolecules *in cellulo* could be behind this fact. Thus, the CPL signal recorded by us from the developed CPL probes based on chiral BINOL-*O*-BODIPY could be birefringently amplified by the local cell environment, helically-chiral organized due to “the Sergeants and Soldiers principle” as discussed above.[34,35]

We have additionally shown the potential of using the readily-accessible CPL-enabling BINOL-*O*-BODIPY scaffold to rapidly design and develop enantiopure small full-organic CPL probes working in different spectral regions. Interestingly, both enantiomeric versions of the probe can be easily obtained by simply selecting the BINOL precursor enantiomer, without the need of using expensive asymmetric syntheses or tedious racemate resolutions. All this make possible easily constructing complementary CPL bioprobes, with complementary CPL signs and colours, paving the way for envisaged multi-CPL-bioimaging experiments based on multi-staining.

Interestingly, the BINOL-*O*-BODIPY-based CPL probes studied herein are not significantly affected by biological diastereomeric interactions resulting in enantiomer-dependent differential bio-accumulation, as it occurred in the seminal lanthanide-complex-based CPL probes.[46] This fact highlights the importance of developing families of structurally-related CPL probes of different nature, molecular, polymeric, full-organic, organometallic, etc., in order to unveil, through comparative CPL-bioimaging experiments, the key roles of chirality in the mechanics and dynamics of the biological processes.

It is also demonstrated that the developed BINOL-*O*-BODIPY-based CPL probes can be activated by near-infrared 2PA, which reinforces their potential as CPL probes. However, these materials still require much improvement in CPL emission (g_{lum} and *CPB*) and 2PA emission (particularly σ^2) to allow MP-CPL-bioimaging.

Overall, we have demonstrated the possibility of CPL-bioimaging using small and full-organic CPL probes. Moreover, the outstanding accessibility, adaptability and workability of the chiral-BODIPY scaffold selected for such a demonstration (BINOL-*O*-BODIPY) support it can be used to advance bioimaging by CPL-LSCM by the design of superior CPL probes. Thus, further studies are now in progress to enhance the level of CPL in this kind of probes, as well as to increase the capability of 2PA-induced emission for MP-CPL-bioimaging. We anticipate that the developments presented herein will open uncharted research avenues for fundamental studies of chiral interactions in the domains of chemistry and molecular biology, aided by the development of future small full-organic CPL bioprobes.

EXPERIMENTAL

Synthesis of (*R*)-BOD1

According to the general methods and general synthetic procedures reported for *rac*-**BOD1**,[22,25] commercial 1,3,5,7,8-pentamethyl-*F*-BODIPY (PM546; 25.0 mg, 0.095 mmol) was reacted with commercial (*R*)-3,3’-dibromoBINOL (84.7 mg, 0.191 mmol) to obtain (*R*)-**BOD1** (61.5 mg, 97%) as an orange solid. $[\alpha]_D^{20}$ −3230 (*c* 0.011, $CHCl_3$). The spectroscopic data agree with those previously reported for *rac*-**BOD1**.[25]

Synthesis of (*S*)-BOD1

According to the above described for (*R*)-**BOD1**, commercial PM546 (25.0 mg, 0.095 mmol) was reacted with (*S*)-3,3’-dibromo-BINOL (84.7 mg, 0.191 mmol) to obtain (*S*)-**BOD1** (60.2 mg,

95%) as an orange solid. $[\alpha]_D^{20}$ +3665 (*c* 0.040, $CHCl_3$). The spectroscopic data agree with those reported for *rac*-**BOD1**.[25]

Synthesis of (*R*)-BOD2

According the above described for (*R*)-**BOD1**, commercial PM546 (29.0 mg, 0.111 mmol) was reacted with (*R*)-3,3'-dicyanoBINOL[47] (44.7 mg, 0.133 mmol) to obtain (*R*)-**BOD2** (35.2 mg, 57%) as an orange solid. $[\alpha]_D^{20}$ −618 (*c* 0.042, $CHCl_3$). The spectroscopic data agree with those reported for *rac*-**BOD2**.[22]

Synthesis of (*S*)-BOD2

According to the above described for (*R*)-**BOD1**, commercial PM546 (30.0 mg, 0.114 mmol) was reacted with (*S*)-3,3'-dicyanoBINOL[47] (46.2 mg, 0.137 mmol) to obtain (*S*)-**BOD2** (40.4 mg, 63%) as an orange solid. $[\alpha]_D^{20}$ +587 (*c* 0.039, $CHCl_3$). The spectroscopic data agree with those reported for *rac*-**BOD2**.[22]

Synthesis of FB2

A mixture of **FB1**[29] (74.6 mg, 0.176 mmol), benzaldehyde (56.1 mg, 0.529 mmol), piperidine (75.0 mg, 0.881 mmol) and acetic acid (52.9 mg, 0.881 mmol) in dry DMF (2 mL) was submitted to microwave irradiation for 1 h at 120 °C. Then, the mixture was diluted with ethyl acetate (30 mL), washed with water (4 × 20 mL) and brine (1 × 20 mL), and dried over anhydrous Na_2SO_4. After filtration and solvent evaporation under reduced pressure, the obtained residue was purified by flash chromatography (silica gel; hexane/AcOEt 9:1→4:6) to obtain **FB2** (71.0 mg, 67%) as a blue solid. R_F = 0.27 (hexane/AcOEt 3:7). ^{1}H NMR ($CDCl_3$, 300 MHz) δ 7.75 (d, *J* = 16.3 Hz, 2H), 7.68-7.60 (m, 4H), 7.50 (d, *J* = 7.7 Hz, 2H), 7.44-7.37 (m, 4H), 7.36-7.21 (m, 6H), 6.65 (s, 2H), 3.77 (t, *J* = 4.6 Hz, 4H), 3.65 (br s, 2H), 2.51 (br s, 4H), 1.45 (s, 6H) ppm. ^{13}C NMR ($CDCl_3$, 75 MHz) δ 152.8 (C), 142.2 (C), 139.1 (C), 137.0 (C), 136.7 (C), 136.4 (CH), 133.5 (C), 130.1 (CH), 129.1 (C), 128.9 (CH), 128.6 (CH), 127.7 (CH), 119.4 (CH), 118.0 (CH), 66.9 (CH_2), 63.1 (CH_2), 53.6 (CH_2), 14.8 (CH_3) ppm. FTIR ν 1538, 1499, 1486, 1445, 1162, 1110, 1069, 990 cm^{-1}.

Synthesis of (*R*)-BOD3

According to the above described for (*R*)-**BOD1**, **FB2** (20.0 mg, 0.033 mmol) was reacted with (*R*)-3,3'-dibromoBINOL (29.6 mg, 0.067 mmol). The reaction residue was purified by column chromatography (neutral alumina; AcOEt) to obtain (*R*)-**BOD3** (21.8 mg, 65%) as a blue solid. R_F = 0.46 (AcOEt). $[\alpha]_D^{20}$ +8600 (*c* 0.002, $CHCl_3$). ^{1}H NMR ($CDCl_3$, 300 MHz) δ 7.95 (s, 2H), 7.50 (d, *J* = 8.1 Hz, 2H), 7.47 (d, *J* = 8.4 Hz, 2H), 7.37 (d, *J* = 8.0 Hz, 2H), 7.06 (ddd, *J* = 8.1, 6.8, 1.2 Hz, 2H), 6.97 (d, *J* = 7.9 Hz, 4H), 6.91 (d, *J* = 16.2 Hz, 2H), 6.84-6.74 (m, 6H), 6.63 (d, *J* = 16.2 Hz, 2H), 6.51 (d, *J* = 7.8 Hz, 4H), 6.48 (s, 2H), 3.76 (t, *J* = 4.6 Hz, 4H), 3.64 (s, 2H), 2.50 (t, *J* = 4.7 Hz, 4H), 1.47 (s, 6H) ppm. ^{13}C NMR ($CDCl_3$, 75 MHz) δ 154.4 (C), 150.8 (C), 141.9 (C), 139.1 (C), 138.6 (C), 136.0 (C), 135.1 (C), 134.7 (C), 134.4 (CH), 132.9 (C), 132.3 (CH), 130.6 (C), 129.9 (CH), 128.8 (CH), 128.1 (CH), 128.0 (CH), 127.5 (CH), 127.0 (CH), 126.9 (CH), 125.2 (CH), 124.7 (CH), 123.3 (C), 119.9 (CH), 119.5 (C), 119.0 (CH), 67.1 (CH_2), 63.3 (CH_2), 53.7 (CH_2), 15.0 (CH_3) ppm. FTIR ν 1546, 1499, 1488, 1446, 1193, 1158, 994 cm^{-1}.

Synthesis of (*S*)-BOD3

Following the synthetic procedure used for (*R*)-**BOD3**, **FB2** (29.0 mg, 0.048 mmol) was reacted with (*S*)-3,3'-dibromoBINOL (43.0 mg, 0.097 mmol) to obtain (*S*)-**BOD3** (28.3 mg, 58%) as a blue solid. $[\alpha]_D^{20}$ −8600 (*c* 0.002, $CHCl_3$). Spectroscopic data agree with the above dated for the *R* enantiomer.

UV-Vis absorption and photoluminescent spectrometry

Photophysical signatures were recorded using the previously described equipment and methods.[22] Likewise, fluorescence quantum yields (ϕ_{em}) were determined using the previously described methodology.[22] Zinc phthalocyanine in toluene with 1% (v/v) of pyridine ($\phi_{R,em}$= 0.30)[48,49] was used as the reference.

CPL spectroscopy

CPL was measured with a home-built (modular) PEM-CPL spectrometer. The excitation source was a broad band (200–1000 nm) laser- driven light source EQ 99 (Elliot Scientific). The excitation wavelength was selected by feeding the broadband light into an Acton SP-2155 monochromator (Princeton Instruments); the collimated light was focused into the sample cell (1 cm quartz cuvette). Sample PL emission was collected perpendicular to the excitation direction with a lens (f = 150 mm). The emission was fed through a photoelastic modulator (PEM) (Hinds Series II/FS42AA) and through a linear sheet polariser (Comar). The light was then focused into a second scanning monochromator (Acton SP-2155) and subsequently on to a photomultiplier tube (PMT) (Hamamatsu H10723 series). The detection of the CPL signal was achieved using the field modulation lock-in technique. The electronic signal from the PMT was fed into a lock-in amplifier (Hinds Instruments Signaloc Model 2100). The reference signal for the lock-in detection was provided by the PEM control unit. The monchromators, PEM control unit and lock-in amplifier were interfaced to a desktop PC and controlled by a Labview code. The lock-in amplifier provided two signals, an AC signal corresponding to (I_L- I_R) and a DC signal corresponding to (I_L + I_R) after background subtraction. The emission dissymmetry factor was therefore readily obtained from the experimental data, as 2 AC/DC.

Spectral calibration of the scanning monochromator was performed using an Hg-Ar calibration lamp (Ocean Optics). A correction factor for the wavelength dependence of the detection system was constructed using a calibrated lamp (Ocean Optics). The measured raw data was subsequently corrected using this correction factor. The validation of the CPL detection systems was achieved using light emitting diodes (LEDs) at various emission wavelengths. The LED was mounted in the sample holder and the light from the LED was fed through a broad band polarising filter and λ/4 plate (Ocean Optics) to generate circularly polarised light. Prior to all measurements, the λ/4 plate and a LED were used to set the phase of the lock-in amplifier correctly. The emission spectra were recorded with 0.5 nm step size and the slits of the detection monochromator were set to a slit width corresponding to a spectral resolution of 0.25 nm. CPL spectra (as well as total emission spectra) were obtained through an averaging procedure of several scans. The CPL spectra have been smoothed using Savitzky-Golay smoothing (polynomial order 5, window size 9 with reflection at the boundaries) to enhance visual appearance; all calculations were carried out using raw spectral data. Analysis of smoothed vs raw

data was used to help to estimate the uncertainty in the stated gem factors, which was typically ±10%.

Emission dissymmetry factor determination

Emission dissymmetry factors (g_{lum}) were determined from the measured L-CPL and R-CPL light intensities according to above-mentioned Eqn. 1.

CPL-laser scanning confocal microscopy

Details of the CPL-LSCM set up are available in publication by Stachelek *et al*.[5] In brief, light from the sample plane of the CPL-LSCM exits the microscope via an output port and into an external CPL analysis module, which is adapted from the rapid CPL spectrometer that we recently reported.[3] First, the waveband of interest is selected by a switchable band-pass filter. Then, an achromatic wave plate converts left and right circularly polarised light into orthogonal linearly polarised states. The light is then split into two analysis pathways by a 50:50 non polarising beam-splitter cube. The two linear polarised light states generated (horizontal and vertical polarisation) corresponding to left or right CPL are selected by a carefully aligned linear polariser, housed in a high-precision computer-controlled rotation mount.[3] Emission intensity of each pixel is quantified in a conventional CPL-LSCM scanned manner by a dedicated high sensitivity avalanche photodiode pair. Whilst each detection arm can operate independently, both components are matched in alignment and specification to enable rapid and simultaneous acquisition of left and right CPL images. Full technical details of the CPL-LSCM system and the applied image processing methodology are provided in the supporting information.

EDCC imaging was realized by subtraction of the simultaneously recorded left-handed CPL image from the right-handed CPL image (and vice versa) using ImageJ software (v 1.49).

MP spectroscopy

Two photon CPL spectroscopy has been achieved by a tunable femtosecond pulsed laser (680–1300 nm, Coherent Discovery TPC, 100 fs, 80 MHz) to an Ocean Optics HR2000Pro (2048-pixel linear CCD Sony ILX5 chip, 200 µm slit, H3 grating, 350–850 nm spectral region) spectrometer. The spectrometer has also been equipped with a perpendicularly mounted 365 nm LED (nichia, 1W) and been operated using custom time resolved detection and accumulation algorithm written in Labview2013 program. In order to eliminate unwanted artefacts associated with stray light from MP excitation each spectrometer have been equipped with a rotating filter wheel (Thor Labs, CFW6) housing an LP420 (Comar Optics, for 365 nm UVLED excitation) and SP650 and SP700 (Edmund Optics, 8472 and 8474 for MP excitation) filters.

Cross section determination

The cross-sections (σ^2) were measured according to established procedures, according to Eqn. 3, where S is sample, R is reference, ϕ is the total emission quantum yield of the compound, C is the concentration, n the refractive index and $F(\lambda)$ is the integrated PL spectrum. Additionally, we have demonstrated that the excitation process is most definitely a two-photon event by recording an excitation power dependence; the resulting line has a slope of two on a logarithmic scale. The cross sections were calculated with reference to Rhodamine B in ethanol.

$$\frac{\sigma_S^2\phi^S}{\sigma_R^2\phi^R} = \frac{C_R n_S F^S(\lambda)}{C_S n_R F^R(\lambda)} \qquad \text{Eqn. 3}$$

Statistics and reproducibility

Where instruments incorporating a scanning monochromator have been used (absorption, emission, and excitation spectra) each sample have been recorded and averaged as triplicate measurements. Spectra, where CCD detectors have been employed, such as CPL spectroscopy, have been measured as an average of a thousand spectra on triplicate samples.

Microscopy images presented herein are representative images of the experiments discussed. Each experiment has been repeated in triplicates and each sample have been recorded and studied recording a minimum of five separate imaging sequences.

Imaging parameters presented, such as brightness and chiroptical contrast have been calculated on each individual imaging sequence according to the protocols above detailed.

ASSOCIATED CONTENT

Supporting Information. Additional figures concerning (chir)optical characterisation and bioimaging experiments, as well as ^{1}H and ^{13}C spectra for new compounds. This material is available free of charge via the Internet at http://pubs.acs.org.

AUTHOR INFORMATION

Corresponding Authors

Robert Pal - Department of Chemistry, Durham University, Stockton Road, Durham DH1 3LE, Durham, United Kingdom.

E-mail: robert.pal@durham.ac.uk.

Santiago de la Moya - Departamento de Química Orgánica, Facultad de, Ciencias Químicas, Universidad Complutense de Madrid, Ciudad Universitaria, s/n, 28040, Madrid, Spain.

E-mail: santmoya@ucm.es.

Authors

Patrycja Stachelek - Department of Chemistry, Durham University, Stockton Road, Durham DH1 3LE, Durham, United Kingdom.

Sergio Serrano-Buitrago - Departamento de Química Orgánica, Facultad de, Ciencias Químicas, Universidad Complutense de Madrid, Ciudad Universitaria, s/n, 28040, Madrid, Spain.

Beatriz L. Maroto - Departamento de Química Orgánica, Facultad de, Ciencias Químicas, Universidad Complutense de Madrid, Ciudad Universitaria, s/n, 28040, Madrid, Spain.

Conflict of Interest

R.P. is inventor on filed patent WO2016174395A1: Light detecting apparatus for simultaneously detecting left-and right-handed circularly polarised light.

Data Availability Statement

The data that support the findings of this study are available from the corresponding author upon reasonable request.

ACKNOWLEDGMENT

R.P. acknowledges support from the Royal Society University Research Fellowship URF\R\191002, H2020-MSCA-ITN-859752

HEL4CHIROLED, BBSRC BB/S017615/1 and BB/X001172/1, and EPSRC EP/X040259/1. P.S. acknowledges support from the Royal Society University Research Fellowship URF\R1\221121. S.d.l.M., B.L.M. and S.S.-B. acknowledge support from Spanish Ministerio de Ciencia e Innovación (MICINN, AEI/10.13039/ 501100011033) PID2020-114755GB-C32. S.S.-B. acknowledges Universidad Complutense de Madrid (UCM) for a pre-doctoral contract (CT58/21-CT59/21).

REFERENCES

[1] Arppe, R.; Sørensen, T. J. Physical unclonable functions generated through chemical methods for anti-counterfeiting. *Nat. Rev. Chem.* **2017**, *1*, 0031.

[2] MacKenzie, L. E.; Pal, R. Circularly polarized lanthanide luminescence for advanced security inks. *Nat. Rev. Chem.* **2021**, *5*, 109-124.

[3] MacKenzie, L. E.; Pålsson, L.-O.; Parker, D.; Beeby, A.; Pal, R. Rapid time-resolved Circular Polarization Luminescence (CPL) emission spectroscopy. *Nat. Commun.* **2020**, *11*, 1676.

[4] De Rosa, D. F.; Stachelek, P.; Black, D. J.; Pal, R. Rapid handheld time-resolved circularly polarised luminescence photography camera for life and material sciences. *Nat. Commun.* **2023**, *14*, 1537.

[5] Stachelek, P.; MacKenzie, L.; Parker, D.; Pal, R. Circularly polarised luminescence laser scanning confocal microscopy to study live cell chiral molecular interactions. *Nat. Commun*. **2022**, *13*, 553.

[6] Arrico, L.; Di Bari, L.; Zinna, F. Quantifying the Overall Efficiency of Circularly Polarized Emitters. *Chem. Eur, J.* **2021**, *27*, 2920-2934.

[7] Grimm, J. B.;Lavis, L. D. Caveat fluorophore: an insiders' guide to small-molecule fluorescent labels. *Nat. Methods* **2022**, *19*, 149-158.

[8] Sánchez-Carnerero, E. M.; Agarrabeitia, A. R.; Moreno, F.; Maroto, B. L.; Muller, G.; Ortiz, M. J.; Moya, S. de la Circularly Polarized Luminescence from Simple Organic Molecules. *Chem. Eur. J.*, **2015**, *21*, 13488-13500.

[9] Bañuelos, J. BODIPY Dye, the Most Versatile Fluorophore Ever? *Chem. Rec.* **2016**, *16*, 335-348.

[10] Mula, S. *BODIPY: A Unique Dye for Versatile Optical Applications* in *Handbook of Materials Science*, *Vol. 1* (Eds: R. S. Ningthoujam, A. K. Tyagi) Springer Nature, Singapore, **2024**, pp. 369–399.

[11] Loudet, A.; Burgess, K. BODIPY Dyes and Their Derivatives: Syntheses and Spectroscopic Properties. *Chem. Rev.*, **2007**, *107*, 4891-4932.

[12] Boens, N.; Verbelen, B.; Ortiz, M. J.; Jiao, L.; Dehaen, W. Synthesis of BODIPY dyes through postfunctionalization of the boron dipyrromethene core. *Coord. Chem. Rev.* **2019**, *399*, 213024.

[13] Gapare, R. L.; A. Thompson, A. Substitution at boron in BODIPYs. *Chem. Commun.* **2022**, *58*, 7351.

[14] Bañuelos, J.; Martín, V.; Gómez-Durán, C. F. A.; Córdoba, I. J. A.; Peña-Cabrera, E.; García-Moreno, I.; Costela, A.; Pérez-Ojeda, M. E.; Arbeloa, T.; Arbeloa, I. L. New 8-Amino-BODIPY Derivatives: Surpassing Laser Dyes at Blue-Edge Wavelengths. *Chem. Eur. J.* **2011**, *17*, 7261-7270.

[15] Harriman, A.; Stachelek, P.; Sutter, A.; Ziessel, R. A bifurcated molecular pentad capable of sequential electronic energy transfer and intramolecular charge transfer. *Phys. Chem. Chem. Phys.* **2015**, *17*, 26175-26182.

[16] Boens, N.; Leen, V.; Dehaen, W. Fluorescent indicators based on BODIPY. *Chem. Soc. Rev.* **2012**, *41*, 1130-1172.

[17] Kaur, P.; Singh, K. Recent advances in the application of BODIPY in bioimaging and chemosensing. *J. Mater. Chem. C* **2019**, *7*, 11361-11405.

[18] Hall, M. J.; Moya, S. de la *BODIPY Based Emitters of Circularly Polarized Luminescence* in *Circularly Polarized Luminescence of Isolated Small Organic Molecules* (Eds: T. Mori) Springer Singapore, **2020**, pp. 117-149.

[19] Sánchez-Carnerero, E. M.; Moreno, F.; Maroto, B. L.; Agarrabeitia, A. R.; Ortiz, M. J.; Vo, B. G.; Muller, G.; Moya, S. de la Circularly Polarized Luminescence by Visible-Light Absorption in a Chiral O-BODIPY Dye: Unprecedented Design of CPL Organic Molecules from Achiral Chromophores. *J. Am. Chem. Soc.* **2014**, *136*, 3346-3349.

[20] Jiménez, J.; Cerdán, L.; Moreno, F.; Maroto, B. L.; García-Moreno, I.; Lunkley, J. L.; Muller, G.; Moya, S. de la Chiral Organic Dyes Endowed with Circularly Polarized Laser Emission. *J. Phys. Chem. C* **2017**, *121*, 5287-5292.

[21] Jiménez, J.; Moreno, F.; Maroto, B. L.; Cabreros, T. A.; Huy, A. S.; Muller, G.; Bañuelos, J.; Moya, S. de la Modulating ICT emission: a new strategy to manipulate the CPL sign in chiral emitters. *Chem. Commun.* **2019**, *55*, 1631-1634.

[22] Jiménez, J.; Prieto-Montero, R.; Serrano, S.; Stachelek, P.; Rebollar, E.; Maroto, B. L.; Moreno, F.; Martínez-Martínez, V.; Pal, R.; García-Moreno, I.; Moya, S. de la BINOL blocks as accessible triplet state modulators in BODIPY dyes. *Chem. Commun.* **2022**, *58*, 6385-6388.

[23] Jiménez, J.; Díaz-Norambuena, C.; Serrano, S.; Ma, S. C.; Moreno, F.; Maroto, B. L.; Bañuelos, J.; Muller, G.; Moya, S. de la BINO-Lated aminostyryl BODIPYs: a workable organic molecular platform for NIR circularly polarized luminescence. *Chem. Commun.* **2021**, *57*, 5750-5753.

[24] Gartzia-Rivero, L.; Sánchez-Carnerero, E. M.; Jiménez, J.; Bañuelos, J.; Moreno, F.; Maroto, B. L.; López-Arbeloa, I.; Moya, S. de la Modulation of ICT probability in bi(polyarene)-based *O*-BODIPYs: towards the development of low-cost bright arene-BODIPY dyads. *Dalton Trans.* **2017**, *46*, 11830-11839.

[25] Jiménez, J.; Prieto-Montero, R.; Maroto, B. L.; Moreno, F.; Ortiz, M. J.; Oliden-Sánchez, A.; López-Arbeloa, I.; Martínez-Martínez, V.; Moya, S. de la Manipulating Charge-Transfer States in BODIPYs: A Model Strategy to Rapidly Develop Photodynamic Theragnostic Agents. *Chem. Eur. J.* **2020**, *26*, 601-605.

[26] Zhang, S.; Wang, Y.; Meng, F.; Dai, C.; Cheng, Y.; Zhu, C. Circularly polarized luminescence of AIE-active chiral O-BODIPYs induced via intramolecular energy transfer. *Chem. Commun.* **2015**, *51*, 9014-9017.

[27] Tsuji, M.; Abuhadba, S.; Chen, A.; Ito, M.; Makhijani, A.; Kuwahara, Y.; Esipova, T.; Mani, T. Red-Colored Circularly Polarized Luminescence from a Benzo-Fused BODIPY-BINOL Complex. *J. Phys. Chem. B* **2023**, 127, 9781-9787.

[28] Hedley, G. J.; Ruseckas, A.; Harriman, A.; Samuel, I. D. W. Conformational Effects on the Dynamics of Internal Conversion in Boron Dipyrromethene Dyes in Solution. *Angew. Chem. Int. Ed.* **2011**, *50*, 6634-6637.

[29] Li, M.; Tian, R.; Fan, J.; Du, J.; Long, S.; Peng, X. A lysosome-targeted BODIPY as potential NIR photosensitizer for photodynamic therapy. *Dyes Pigments* **2017**, *147*, 99-105.

[30] Lu, H.; Mack, J.; Yang, Y.; Shen, Z. Structural modification strategies for the rational design of red/NIR region BODIPYs. *Chem. Soc. Rev.* **2014**, *43*, 4778-4823.

[31] Carr, R.; Puckrin, R.; McMahon. B. K.; Pal, R.; Parker, D.; Pålsson, L.-O. Induced circularly polarized luminescence arising from anion or protein binding to racemic emissive lanthanide complexes. *Methods Appl. Fluoresc.* **2014**, *2*, 024007.

[32] Frawley, A. T.; Pal, R.; Parker, D. Very bright, enantiopure europium(III) complexes allow time-gated chiral contrast imaging. *Chem. Commun.* **2016**, *52*, 13349-13352.

[33] Prins, L. J.; Timmerman, P.; Reinhoudt, D. N. Amplification of Chirality: The "Sergeants and Soldiers" Principle Applied to Dynamic Hydrogen-Bonded Assemblies. *J. Am. Chem. Soc.* **2001**, *123*, 10153-10163.

[34] Green, M. M.; Reidy, M. P.; Johnson, R. D.; Darling, G.; O'Leary, D. J.; Willson, G. Macromolecular stereochemistry: the out-of-proportion influence of optically active comonomers on the conformational characteristics of polyisocyanates. The sergeants and soldiers experiment. *J. Am. Chem. Soc.* **1989**, *111*, 6452-6454.

[35] Palmans, A. R. A.; Vekemans, J. a. J. M.; Havinga, E. E.; Meijer, E. W. Sergeants-and-Soldiers Principle in Chiral Columnar Stacks of

Disc-Shaped Molecules withC3 Symmetry. *Angew. Chem. Int. Ed. English* **1997**, *36*, 2648-2651.

[36] Anderson, T. W.; Sanders, J. K. M.; Pantoş, G. D. The sergeants-and-soldiers effect: chiral amplification in naphthalenediimide nanotubes. *Org. Biomol. Chem.* **2010**, *8* 4274-4280.

[37] Wang, Y.; Fang, H.; Tranca, I.; Qu, H.; Wang, X.; Markvoort, A. J.; Tian, Z.; Cao, X. Elucidation of the origin of chiral amplification in discrete molecular polyhedral. *Nat. Commun.* **2018**, *9*, 488.

[38] Denk, W.; Strickler, J. H.; Webb, W. W. Two-Photon Laser Scanning Fluorescence Microscopy. *Science* **1990**, *248*, 73-76.

[39] Denk, W.; Svoboda, K. Photon Upmanship: Why Multiphoton Imaging Is More than a Gimmick. *Neuron* **1997**, *18*, 351-357.

[40] Liu, D.; García-López, V.; Gunasekera, R. S.; Nilewski, L. G.; Alemany, L. B.; Aliyan, A.; Jin, T.; Wang, G.; Tour, J. M.; Pal, R. Near-Infrared Light Activates Molecular Nanomachines to Drill into and Kill Cells. *ACS Nano* **2019**, *13*, 6813-6823.

[41] Yang, J.; Rousselin, Y.; Bucher, L.; Desbois, N.; Bolze, F.; Xu, H.-J.; Gros, C. P. Two-Photon Absorption Properties and Structures of BODIPY and Its Dyad, Triad and Tetrad. *Chempluschem* **2018**, *83*, 838-844.

[42] He, G. S.; Tan, L.-S.; Zheng, O.; Prasad, P. N. Multiphoton Absorbing Materials: Molecular Designs, Characterizations, and Applications. *Chem. Rev*. **2008**, *108*, 1245-1330.

[43] Didier, P.; Ulrich, G.; Mély, Y.; Ziessel, R. Improved push-pull-push E-Bodipy fluorophores for two-photon cell-imaging *Org. Biomol. Chem.* **2009**, *7*, 3639-3642.

[44] Barros, L. W. T.; Cardoso, T. A. S.; Bihlmeier, A.; Wagner, D.; Kölmel, D. K.; Hörner, A.; Bräse, S.; Cruz, C. H. B.; Padilha, L. A. Two-photon absorption in a series of 2,6-disubstituted BODIPY dyes. *Phys. Chem. Chem. Phys.* **2017**, *19*, 21683-21690.

[45] Dipold, J.; Romero, E. E.; Donnelly, J.; Calheiro, T. P.; Bonacorso, H. G.; Iglesias, B. A.; Siqueira, J. P.; Hernandez, F. E.; De Boni, L.; Mendonca, C. R. Two-photon absorption properties of BODIPY-like compounds based on BF 2 –naphthyridine complexes. *Phys. Chem. Chem. Phys.* **2019**, *21*, 6662-6671.

[46] Frawley, A. T.; Linford, H. V.; Starck, M.; Pal, R.; Parker, D. Enantioselective cellular localisation of europium (III) coordination complexes. *Chem. Sci.* **2018**, *9*, 1042-1049.

[47] Turner, H. M.; Patel, J.; Niljianskul, N.; Chong, J. M. Binapthol -Catalyzed Asymmetric Conjugate Arylboration of Enones. *Org. Lett.* **2017**, *147*, 99-105.

[48] Vicent, P. S.; Voigt, E. M.; Rieckhoff, K. E. Phosphorescence and Fluorescence of Phtalocyanines. *J. Chem. Phys.* **1971**, *55*, 4131-4140.

[48] van Leeuwen, M.; Beeby, A.; Fernandes, I.; Ashworth, S. H. The photochemistry and photophysics of a series of alpha octa(alkyl-substituted) silicon, zinc and palladium phthalocyanines. *Photochem. Photobiol. Sci.* **2014**, *2014*, 62-69.

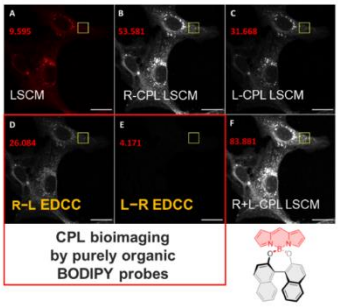
A
9.595
LSCM
B
53.581
R-CPL LSCM
C
31.668
L-CPL LSCM
D
26.084
R-L EDCC
E
4.171
L-R EDCC
F
83.881
R+L-CPL LSCM
CPL bioimaging
by purely organic
BODIPY probes